Catalysis Today 257 (2015) 177–184

Contents lists available at ScienceDirect

Catalysis Today

journal homepage: www.elsevier.com/locate/cattod

Hydrogen-rich gas production from algae-biomass by low temperature catalytic gasification

M.R. Díaz-Rey [a], M. Cortés-Reyes [a], C. Herrera [a], M.A. Larrubia [a], N. Amadeo [b], M. Laborde [b], L.J. Alemany [a,*]

[a] Departamento de Ingeniería Química, Facultad de Ciencias, Campus de Teatinos, Universidad de Málaga, Málaga E-29071, Spain
[b] Laboratorio de Procesos Catalíticos, Departamento de Ingeniería Química, Facultad de Ingeniería Ciudad Universitaria, 1428 Buenos Aires, Argentina

ARTICLE INFO

Article history:
Received 28 February 2014
Received in revised form 11 April 2014
Accepted 16 April 2014
Available online 1 July 2014

Keywords:
Algal biomass
Thermocatalytic conversion
Ni-based catalysts

ABSTRACT

H_2 rich gas produced from *Scenedesmus almeriensis* biomass residue after lipidic extraction by low temperature catalytic gasification is addressed. The pyrolysis–gasification behavior under different atmospheres (CO_2/He, H_2O/He and $CO_2 + H_2O$/He) were investigated using thermal gravimetric analysis. The conversion of the biomass takes place into three stages, according to its composition and corresponding to: loose of water bonded (30–200 °C), major pyrolysis involving devolatilization (200–500 °C) and decomposition of bio-char produced (500–800 °C). The calculated apparent activation energy for the main pyrolysis stage was 97 kJ mol^{-1}. Ni-based supported alumina catalysts (Ni, Ni–Pt and Ni–Rh) were prepared by impregnation. The catalyst influence on the final gas composition as well as in its HHV determined in mixed $CO_2 + H_2O$/He gasification carried out in a double fixed bed reactor configuration with the catalyst located in the second bed upstream. Parallel and secondary reactions as reforming of tar and char together with WGS and Boudouard also take place favoring gas fraction yield with a value close to 0.3 Nm^3 of gas per kg of biomass. The catalytic role of Ni–Pt/Al_2O_3 catalyst in further reforming of the gas resulting from the gasification improves H_2 content even at low temperature interval (600–700 °C).

1. Introduction

The conversion of microalgae biomass to energy and valuable chemicals are gaining significant attention over the last few years. Considering a very high photosynthetic effectiveness, a fast rate biomass growth even under nutrients limitations, the resistance to various types of contaminants, the capacity of making changes in the metabolic routes favoring different final biomass composition and the possibility of land management that cannot be used for other purpose, microalgae appears as a competition to typical energetic crops [1–4]. Most of research works published so far have been focused on the biodiesel production technologies based on lipids that are accumulated in large quantities in cells of algae [5]. In contrast, the use of microalgae as potential substrates in processes of biogas production has recently been addressed.

Biomass-to-fuel (liquid or gas) conversion technologies can be classified into two categories, namely biochemical and thermochemical [6]. Thermochemical technologies utilize high temperature and or catalysts to produce char, oil and gas. There are two major thermochemical reaction pathways: gasification and pyrolysis. Pyrolysis processes also heat biomass in the absence of oxygen, but at a relatively lower temperature (450–600 °C). The main product of the pyrolysis process is a crude-like liquid known as pyrolysis oil, while gas and charcoal are also produced. Depending on the length of the reaction time, there are slow pyrolysis, intermediate pyrolysis, and fast pyrolysis. Fast pyrolysis is often adopted because the yield of pyrolysis oil is maximized [7]. In the gasification pathway, the biomass resources are fed into a gasifier, where they are thermally decomposed with limited or no oxygen, and then oxidized to yield a raw syngas, which is primarily a mixture of hydrogen and carbon monoxide.

Several researches have been conducted on biomass gasification [8] for improving the producer gas composition (H_2, CO, CO_2, CH_4 and C_nH_m), obtaining a gas with considerable LHV, reducing the tar and char content of the effluent stream and enhancing the gas yield, cold gas efficiency and carbon conversion. It is very difficult to meet all these performance indexes at their desirable values at the same time, for example, increasing the bed temperature to reduce the tar concentration will significantly reduce the LHV and cold gas efficiency. The main reactions taking place during the conversion

* Corresponding author. Tel.: +34 952 13 1919; fax: +34 952 13 1919.
E-mail address: luijo@uma.es (L.J. Alemany).

http://dx.doi.org/10.1016/j.cattod.2014.04.035
0920-5861/

Table 1
Main gasification reaction.

	ΔH_r° (kJ mol^{-1})	
Devolatilization		
Biomass + Q → Carbonaceous residue (char) + tars + oils + gases (CO, CO_2, H_2, CH_4, C_nH_m)	Endothermic	(1)
Secondary cracking and reforming	Endothermic	
Tars + H_2O ↔ CO, H_2		(2)
Tars + Q → char + gases (CH_4, H_2, C_nH_m)		(3)
Combustion		
$C + O_2 \rightarrow CO_2$	−394	(4)
$C + 1/2O_2 \rightarrow CO$	−123	(5)
$CO + 1/2O_2 \rightarrow CO_2$	−283	(6)
$H_2 + 1/2O_2 \rightarrow H_2O$	−242	(7)
Gasification		
Char gasification		
$C + H_2O \rightarrow CO + H_2$, Water gas reaction	131	(8)
$C + CO_2 \rightarrow 2CO$, Boudouard reaction	171	(9)
Water gas shift reaction (WGS)		
$CO + H_2O \leftrightarrow CO_2 + H_2$	−41	(10)
Hydrocarbons reforming reactions	Endothermic	
$C_nH_m + nCO_2 \rightarrow m/2H_2 + 2nCO$		(11)
$C_nH_m + nH_2O \rightarrow nCO + (m/2 + n)H_2$		(12)
Methanations		
$CO_2 + 4H_2 \rightarrow CH_4 + H_2O$	−165	(13)
$CO + H_2 \leftrightarrow CH_4 + H_2O$	−205	(14)
Cracking reactions		
$C_nH_m + (2n - m/2)H_2 \rightarrow nCH_4$	Exothermic	(15)

process are covered in Table 1 [9,10]. The presence of catalyst in the bed material during biomass gasification promotes several chemical reactions which affect the composition and heating value of the producer gas. It also reduces the tar yield and prevents solid agglomeration tendency of the bed [11]. Ni or Co based catalysts that are used for methane and other higher hydrocarbons reforming reaction facilitate the cracking of the biomass heavy fractions, reducing tar formation. In addition, 700–800 °C are required to promote CO and H_2 formation [12,13].

A cheaper, long life and sulphur-resistant material is desirable. In addition, most commercial Ni catalysts present a moderate to rapid deactivation due to surface carbon deposition originated from gasification and/or reforming reaction [14]. Noble metal catalysts (Rh or Pt) showed lower deactivation as well as superior catalytic activity in the conversion of almost all the tar and char at unusually low temperatures (500–700 °C) [15] but their costs are elevated. This paper presents the results of the low temperature catalytic gasification of *Scenedesmus almeriensis* biomass after lipids extraction (*Sc*). In this study, the pyrolysis of the *Sc* in different atmosphere was studied by ATD-TG-MS and a two-stage technology: pyrolysis and gasification processes were conducted in a doubled-fixed bed reactor, under non isothermal and isothermal regime using $CO_2 + H_2O$/He and Ni-noble metal supported catalysts.

2. Experimental

2.1. Biomass characterization

The microalga *S. almeriensis* (*Sc*) was supplied by the FYBOA Investigation Group from the Department of Ecology of the University of Malaga as a dry green powder with particle size <250 μm. Biomass was obtained after lipid extraction in a conventional Soxhlet extraction equipment using hexane as solvent. Proximate and ultimate analyses were performed to determine the composition of the biomass. The elemental compositions (C, H, N, O and S) of the biomass after lipids extraction, tarry substances and char were determined with an *Elemental Analyzer Perkin-Elmer 2400 CHN*. Higher heating value (HHV) was also calculated according to Mahinpey et al. [16], based on the elemental analysis. Proximate analysis included measurement of moisture content, volatile matter, fixed carbon and ash. The moisture content of the biomass was determined by drying the samples in a furnace at 105 °C until no further weight change was observed. The volatile matter measuring was performed in *T.A. Instrument SDT Q600* thermal analyzer. Ash content was carried out according to Sluiter et al. [17]. Fixed carbon content was calculated by different the percentages of volatile matter, moisture content and ash to 100%. The content of lipid was determined by gravimetry. Total protein was determined according to the procedure of Kebelman et al. [18]. The results of proximate, compositional and elemental analysis of *Sc* biomass are shown in Table 2.

2.2. Catalysts preparation

Monometallic Ni/Al_2O_3 and bimetallic $Pt–Ni/Al_2O_3$ and $Rh–Ni/Al_2O_3$ catalysts were prepared by simultaneous incipient wetness impregnation of the support with aqueous solutions of $Ni(NO_3)_2{\cdot}6H_2O$, $Pt(NH_3)_2(NO_2)_2$ or $Rh(H_2O)(OH)_{3-y}(NO_3)_y$ ($y = 2–3$) as precursors of Ni, Pt or Rh, respectively. In detail, monometallic Ni (4 at nm^{-2}; $4Ni/Al_2O_3$), as well as bimetallic noble metal–Ni catalysts with 4 at nm^{-2} of Ni and a low amount of Pt (0.4 at nm^{-2}; $0.4Pt–4Ni/Al_2O_3$) or Rh (0.04 at nm^{-2}; $0.04Rh–4Ni/Al_2O_3$) were prepared. After impregnation the catalysts were kept in stagnant air at 383 K overnight and then treated in air at 1073 K for 2 h (10 K min^{-1}). A synthesized nanofibrous γ-Al_2O_3 was employed as support ($A_{BET} = 100\ m^2\ g^{-1}$ and $V_P = 1\ cm^3\ g^{-1}$), the synthesis procedure and characterization has been already reported in [19,20]. The synthesized catalysts, Ni, Pt or Rh content and their identification are summarized in Table 3.

The physico/chemical properties of fresh Ni/Al_2O_3, $Ni–Pt/Al_2O_3$ and $Ni–Rh/Al_2O_3$ catalyst were well characterized by various characterization methods, which could be found in our previous studies [20,21]. We stated that in the fresh catalytic systems, the presence of noble metal (Rh or Pt) even in very low loadings inhibits the migration of part of the Ni to form $NiAl_2O_4$, enhancing the Ni accessible sites. A strong noble metal–Ni interaction was also reported that stabilizes the Ni species, promoting its reducibility and the better dispersion of Ni. We have also investigated coke deposition over $Pt–Ni/Al_2O_3$ and $Rh–Ni/Al_2O_3$ (with low noble metal loadings) in mixed ($CO_2 + H_2O$) methane reforming compared to Ni/Al_2O_3 catalysts. It was also been informed the formation of PtNi alloy which the surface enriched in Pt. Low amounts of Pt or Rh in Ni-based catalysts allow an improvement in the reaction stability as well as in the selectivity toward H_2 and CO instead toward coke.

2.3. Reactivity

2.3.1. Thermogravimetric-MS analysis

The study of the pyrolysis–gasification of *Sc* biomass was firstly carried out in a TGA system (*T.A. Instrument SDT Q600*). Samples consisting of 10 mg of biomass and silicon carbide or biomass and catalyst (9/1 wt.) loaded into an alumina crucible were heated from 30 to 800 °C with a heating rate of 10 K min^{-1} under 20% gasifying agent/He atmosphere. H_2O, CO_2 or $H_2O + CO_2$ were used as gasifying agent. Water vapor (1%, v/v) was generated by saturation of carrier gas at 9 °C. A mass spectrometer (QMS 200 Pfeiffer Vacuum Prisma™) was coupled to analyze the gas products distribution. All wirings were properly thermally insulated to avoid condensation of flue gasses. The *m*/*z* signals of H_2 (2), CH_4 (15), H_2O (18),

Table 2
Proximate, elemental and compositional analysis of the dry microalgae after lipid extraction.

Proximate analysis (wt.%)				Compositional analysis (wt.%)		
Moisture	Ash	Volatile matter	Fixed carbon[a]	Proteins	Lipids	Carbohydrates[a]
4	14.5	70	11.5	58.9	3.6	19

Ultimate analysis (wt.%)					HHV (MJ kg^{-1})
C	H	N	O	S	
41.78	6.81	7.94	42.93	0.55	17.6

[a] Calculated by difference:
Fixed carbon (%) = 100-Moisture-Ash-Volatile matter.
Carbohydrate (%) = 100-Lipids-Proteins-Ash-Moisture.

C_2H_2 (26), C_2H_4 (27), CO (29), C_2H_6 (30), H_2S (34), CO_2 (44) and SO_2 (64) were followed. The signals were normalized with respect to the maximum intensity of each signal during each experiment. Special attention was paid in representing CO_2 and H_2O signals of the gas evolved products by subtracting the flow rate at the inlet from those signals at the outlet.

2.3.2. Doubled fixed bed reactor configuration-MS

Gasification experiments were performed in a quartz tube reactor in 20% CO_2 + H_2O/He atmosphere (S/C = 1/9). The total gas flow was 100 ml min^{-1} using 40 mg of biomass and 4 mg of catalyst or silicon carbide located upstream and separated by a thin layer of quartz particles (GHSV = 44,000 h^{-1}, at 1 atm and 293 K). A mass spectrometer (*QMS 200 Pfeiffer Vacuum Prisma*^{TM}) was coupled to analyze the gas-off products distribution taking into account the experimental and methodological procedures described earlier. The catalyst was reduced by H_2 at 600 °C for 2 h.

2.3.3. Two stages fixed bed reactor-GC under isothermal conditions

Isothermal reactivity experiments were carried out in a dual-fixed bed reaction system at atmospheric pressure in a temperature range between 400 and 700 °C using 40 mg of catalyst (250–420 μm) and 400 mg of dry and defatted biomass. The reactor contained the primary bed for pyrolysis of biomass and accumulation of solids products such as char and ash. The products in the gas phase (including tar) were introduced in the secondary catalytic bed. The total gas flow rate was kept constant at 50 N cm^3 min^{-1} (He/CO_2 = 45/5) and passed through a saturator containing liquid water. The vapor stream of the saturator was estimated by the vapor pressure of water at 9 °C. The space velocity and the contact time were 750 h^{-1} and 0.36 $g_{biomass+catalysts}$ h mol^{-1}, respectively; operating under plug flow conditions. Preliminary reactivity tests with different catalyst particle sizes and dilutions, measuring the radial and axial temperatures at different points, were performed to confirm the non-existence of heat or mass transfer limitations. Before reaction, catalysts were activated in situ with H_2 (20% in H_2, 15 N cm^3 min^{-1}) at 600 °C during 2 h. The reaction temperature was measured with a thermocouple placed in the reactor bed. In order to separate any liquid from the effluent gas, it was successively passed through a 2-propanol condenser tube. The non-condensable gas composition was analyzed by a coupled gas chromatograph, *Agilent 4890 D*, equipped with TCD and FID detectors. At the end of each run, the remaining solid residue (char + ash) was carefully removed from the reactor, weighed and analyzed.

3. Results and discussion

3.1. Thermogravimetric study of gasification of S. almeriensis biomass

Fig. 1A shows the integral and differential thermograms (TGA-DTG) of the Sc microalgae biomass for different gasifying agent, considering a biomass particle size of <250 μm, 20% (v/v) gas/He, a heating rate of 10 °C min^{-1} and 10 mg of initial sample weight (9:1 wt% biomass:SiC). The DTG curves associated with the decomposition of biomass can be resolved into peaks associated to the different stages of biomass conversion. As were reported by other authors [18,22–25] the conversion of microalgae took place into three stages. The first stage occurred in the 30–200 °C interval representing the 8% of weight-lost, which correspond to the loose of free water and water loosely bound to biomolecules. The second stage of decomposition, ranging from 200 to 500 °C with the major weight lost (60%), is associated to major pyrolysis in which devolatilization takes place, involving different complex processes according to the overlapping maxima detected in the DTG curves corresponding to thermal cracking of protein and carbohydrates (320 °C) and lipids non-extracted (430 °C) from the biomass. The temperature range for the pyrolysis of *Sc* was much lower than that for the pyrolysis of lignocellulosic biomass (450–650 °C). Finally, the third stage from 500 to 800 °C correspond to the ulterior decomposition of the forming bio-char. At the end of this stage between 25 and 30 wt.% of solid residue was registered (TGA) including also the unalterable SiC initially loaded to the crucible which remained undecomposed. This residue is composed by fixed carbon and ash, as were shown in the proximate analysis (Table 2). Therefore, the behavior of the biomass conversion may be explained based on the characteristics of the components which comprise the biomass, taking into account that major components (Table 2) were proteins (58.9 wt.%) and carbohydrates (19 wt.%). Only small differences in the curves are detected and in particular under CO_2 + H_2O mixed atmosphere, the DTG peak height of the main devolatilization process increased and the amount of solid after TGA slightly decreased. The calculated apparent activation energy for the main pyrolysis stage based on the Arrhenius equation is 97 kJ mol^{-1}.

Table 3
Theoretical metal content of the catalysts.

Catalyst	Metal density (at nm^{-2})		Metal content (wt.%)	
	Ni	Pt/Rh	Ni	Pt/Rh
4Ni/Al_2O_3	4	–	10	–
0.4Pt–4Ni/Al_2O_3	4	0.4	10	4
0.04Rh–4Ni/Al_2O_3	4	0.04	10	0.2

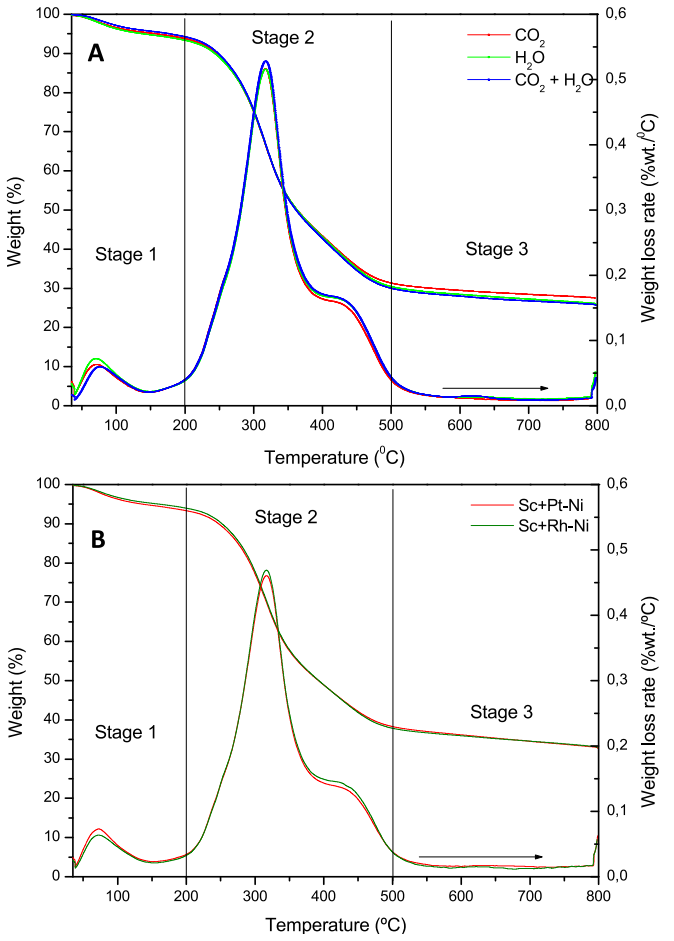

Fig. 1. (A) Thermogravimetric and differential thermogravimetric (TG-DTG) analysis of the SC biomass under different gasifying agents. 20%/He. (B) Thermogravimetric and differential thermogravimetric (TG-DTG) analysis of the Sc biomass using Pt–Ni/Al_2O_3 and Rh–Ni/Al_2O_3.

Many studies have dealt the effect of CO_2, steam or $CO_2 + H_2O$ mixed atmosphere in the gasification of biomass and char. According to Florin and Harris [26], water vapor has been identified as a catalysts for the char formation mechanism, enhancing the concentration of H_2 during the char gasification due to the occurrence of the water gas shift reaction. On the other hand, Zhang et al. [27] reported that the pyrolysis in CO_2 atmosphere produced less char than in the other atmospheres by two main mechanism: the CO_2 reaction with the active volatiles or with the biomass char. Chen and Lin [28] reported that high CO_2 fraction in gasifying agent generally resulted in low H_2 yield and high CO yield. This affirmation was also confirmed by Prabowo et al. [29] which also inform about the positive effect of $CO_2 + H_2O$ mixing ratio on the thermal efficiency of the gasification process compared to N_2 assisted pyrolysis in syngas production. In our currents reaction conditions, the behavior of biomass gasification could be also explained according to the reactions taking place once the primary devolatilization products have been released, including cracking, steam or CO_2 reforming and water gas shift reaction, promoted by the gas feed composition and modifying the gas-off composition.

The influence of Pt–Ni/Al_2O_3 and Rh–Ni/Al_2O_3 catalysts was investigated under $CO_2 + H_2O$/He atmosphere (Fig. 1B) in the TGA-DTG analysis. It can be observed that the mass loss profiles are very closed and similar to that obtained without catalyst. Three sequential stages were also denoted taking place in the same temperature intervals presenting identical temperature maxima. In addition, a deviation of 5% in the weight of the solid residue was registered in comparison with the amount of solid residue resulting from TGA runs in absence of catalysts. This solid residue (25–30 wt.%) comprised the non converted biomass and the ash produced in addition to the catalysts initially loaded. These results could suggest that Ni-based catalysts are not directly involved in the main gasification processes. However, secondary reaction such as reforming of condensable compounds and light hydrocarbons can be promoted, adjusting the final gas composition. Nickel catalysts were also informed to act as a catalyst of the tar or heavy fractions produced in the gasification process [30].

Fig. 2 shows the MS curves of the gaseous products (H_2, CO, CO_2, CH_4, C_2H_4, C_2H_6, H_2S and SO_2) released during the gasification process. H_2S and SO_2 are associated to the degradation of sulphur contained in biomass (S content = 0.55 wt.% from CHNOS, Table 2). Besides H_2O, CO and CO_2, detected before 200 °C due to the moisture content in *Sc* biomass, gas products were primarily detected during the second degradation step. Fig. 2A shows the MS curves of the gas products evolved using H_2O/He as gasifying agent. CO_2 was mainly generated during this first pyrolysis step due to the degradation (cracking or reforming) of the carboxyls groups and proteins as was already reported [23]. No N-containing compounds were detected in the gas products despite the high nitrogen content in the Sc microalgae biomass (7.94wt.%, from CHNOS analysis), so N could be possibly present in the tar and/or solid residue obtained after TG runs. CO, CH_4, C_2H_4, C_2H_6 and H_2S and SO_2 were also majorly produced in the last pyrolysis stage (>400 °C) increasing due to the decomposition of the solid produced when the rate of CO_2 formation was decreased. On the other hand, the H_2 evolution occurred also during devolatilization but it is increased mainly in the third step >600 °C enhancing its intensity when CH_4 and C_2H_4 signals decreased (650 °C). This fact joint to the evolution of the gas product distribution indicates that secondary as water gas (Eq. (8)), water gas shift (Eq. (10)) and methane steam reforming ($CH_4 + H_2O \rightarrow CO + 3H_2$) were predominant at higher temperature [23,26]. H_2 formation observed at high temperature can be also attributed to tar steam reforming (Eq. (2)) and thermal cracking (Eq. (3)).

Fig. 2B shows the MS curves of the gas products evolved using CO_2/He as gasifying agent. CO_2 signal was not represented since it was no possible to give a reliable result on the CO_2 yield because the amount of CO_2 produced is much smaller than the amount of CO_2 fed. Gas products (CO, H_2S, C_2H_6 and CH_4) begin to release at temperature >400 °C. It is also observable that H_2 evolution during devolatilization is negligible as results from the lessen role of water gas shift reaction (Eq. (10)) and H_2 consumption by the presented CO_2 through the backward of water gas shift reaction according to [29] CH_4 present its maximum signal at 600 °C and begin to decrease then in favor of H_2 production. It has been reported that CO_2 gasification generally has lower reaction rates than steam gasification [31], but also increases the production of CO and reduces the H_2 .At temperatures above 650 °C Boudouard reaction (Eq. (9)) takes place, promoting CO formation.

Under the mixed atmosphere (Fig. 2C) gas evolution observed showed the same trend observed for H_2O/He atmosphere but with the following differences: H_2 evolution was continuously observed up to 500 °C coinciding the maximum in CO_2 signal. Hydrogen was released at rather high temperatures possibly because it was formed basically via cracking the released volatiles and reforming reactions, which requires higher temperatures. CO evolution was observed above 320 °C with an increasing trend with temperature. Besides, CO_2 consumption was more apparently observed during the third stage of gasification, due to char reaction (Eq. (9)) occurring together with the forward water gas shift reaction (Eq. (10)).

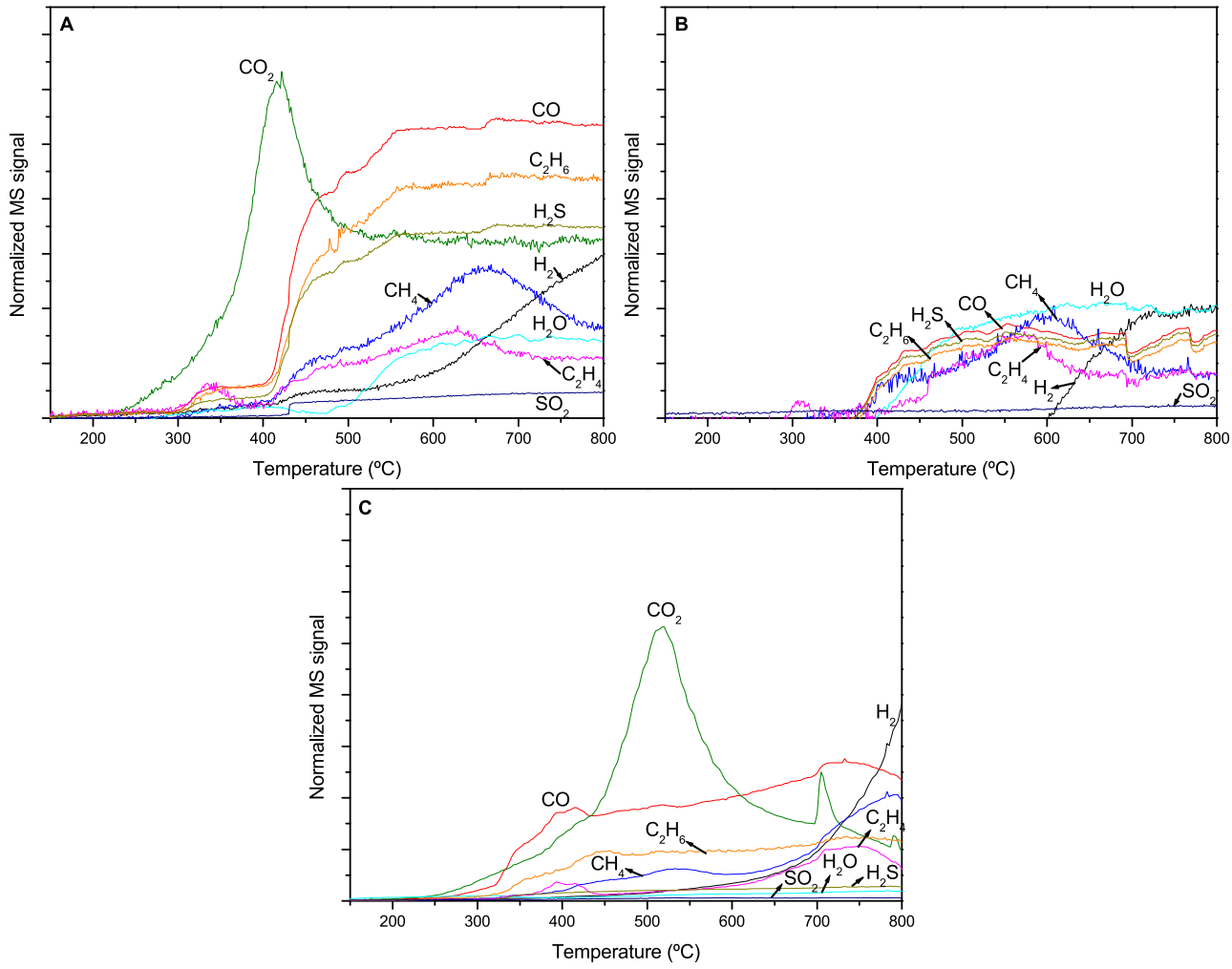

Fig. 2. Normalized mass spectra of gas products corresponding to the different stages of gasification process under (A) CO_2/He, (B) H_2O/He and (C) $CO_2 + H_2O$/He.

3.2. *Catalytic gasification of* S. almeriensis *biomass in* $CO_2 + H_2O$/He *atmosphere*

3.2.1. *Non isothermal two-stages fixed bed-MS*

Two-stages fixed-bed reactor was used to investigate the gasification process of *S. almeriensis* defatted biomass. The test in a quartz fixed bed reactor was carried out in a $H_2O + CO_2$/He atmosphere under gradual heating from room temperature to 800 °C at 10 °C min^{-1}. The sample of biomass (after lipids extraction) was 0.4 mg and the carrier gas flow rate was 100 ml min^{-1}. The effluent gas product was analyzed using a mass spectrometer. In order to investigate the effect of catalysts formulation in the gas product distribution, Ni-based and modified with Pt or Rh supported on alumina catalysts were studied.

Fig. 3 shows the MS profiles of Sc biomass under $H_2O + CO_2$/He atmosphere using these different catalysts. H_2, CH_4, CO, CO_2, C_2H_x, H_2S and SO_2 were registered as the main gases, similar to the detected gas composition in the TG-MS experiments. H_2O was also followed but it did not show appreciable changes with increasing temperature. It can be clearly seen that for all tests, at about 250 °C the gas products, except H_2, were started to generate. This temperature coincides with the initial pyrolysis, which it has been described in TG-MS tests. As can be observed in Fig. 3A, Ni/Al_2O_3 catalyst has a great influence on gas composition, which favors the H_2 production at lower temperatures. So, a high increase in H_2 signal is observed above 700 °C. Furthermore, significant increases of evolution of CO, CO_2, C_2H_4 and CH_4 at lower temperatures were observed with the addition of nickel catalyst. CH_4 and C_2H_4 maxima signals were detected close to 760 and 720 °C, respectively, lower temperatures in comparison with the non-catalytic gasification process. From all the above results, it could be considered that the Ni/Al_2O_3 catalyst accelerated effectively water–carbon reaction (Eq. (8)), reverse water–gas shift reaction (Eq. (10)) and steam reforming of CH_4 or tar cracking (Eq. (3)) [32]. As can be seen from Fig. 3, the syngas content increases significantly with the addition of the Ni/Al_2O_3 catalyst, the content of H_2 increases with increasing temperature, while the CO content increases initially and then decreases. This is the most important fact observed and is attributed to the presence of Ni-catalyst.

In Fig. 3B it is registered that the incorporation of Rh to the catalyst formulation promotes the production of H_2 at lower temperatures. So, comparing the formation rates of H_2, CO and CO_2 for the non-catalytic gasification it is possible to detect that the H_2 proportion is superior, with a less formation of CO and CO_2. This effect is associated to Rh–Ni centers that provoke a lower amounts of lights hydrocarbons due to enhancement of reforming reaction. Rh was reported to allow higher activation of H_2O and CH_4 giving higher methane conversion in the DRM + H_2O reaction of methane [20].

Pt–Ni/Al_2O_3 catalyst (Fig. 3C) exhibited similar gas evolution profiles, except for H_2. In comparison to Ni and Rh–Ni catalytic systems, the Pt–Ni catalyst promotes the maximum production of

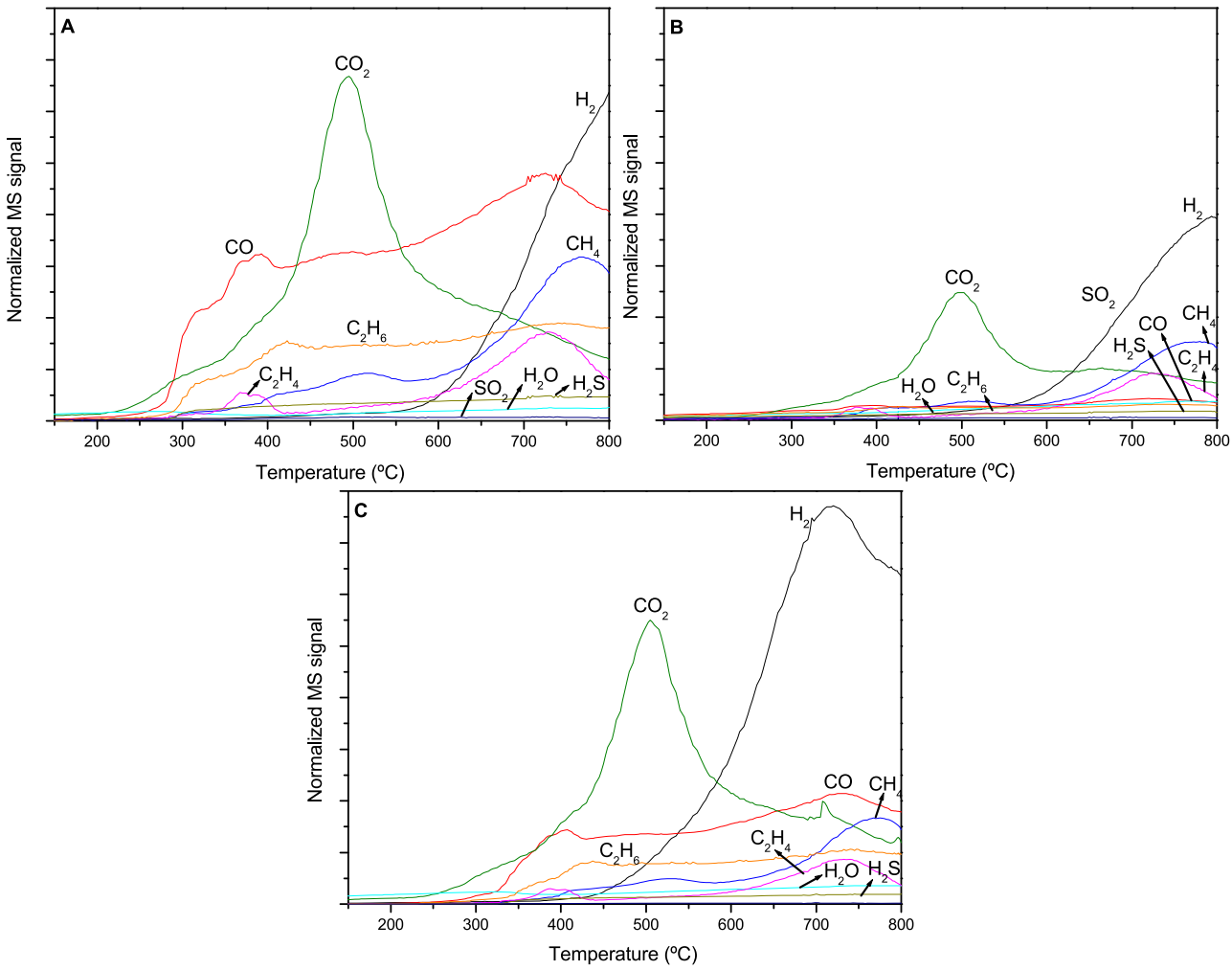

Fig. 3. Normalized MS signal of the gas products in the catalytic gasification of Sc biomass under $CO_2 + H_2O$/He atmosphere under non isothermal test in the double fixed bed reactor coupled to MS. (A) Ni/Al_2O_3(N), (B) $Rh–Ni/Al_2O_3$ and (C) $Pt–Ni/Al_2O_3$.

H_2 at lower temperatures, it reached a peak at 700 °C. Also, when $Pt–Ni/Al_2O_3$ is used as catalyst, lower amount of undecomposed tarry materials adhered to the wall of the reactor was observed. This indicates that the catalyst favors the tar cracking into little molecules (H_2, CO, CO_2) and, as consequence, the gas yield increases. Furthermore, is able to reduce the H_2S content. Thus, from the comparison with the others catalysts tested, it was noted that the effect of Pt incorporation was more effective than Rh, especially at above 650 °C. This results coincide with the reported by Nishiwaka et al. for the additive effect of noble metals to the $Ni/CeO_2/Al_2O_3$ [33].

3.2.2. Isothermal double fixed bed reactor-GC

In this section is analyzed the coupling of pyrolysis–gasification processes performed in a double fixed bed configuration coupled to a gas chromatograph and operating in batch mode, analyzing how temperature and reaction time affect not only the gas yield and its distribution but also the composition of tars and char obtained. Tests (20%($H_2O + CO_2$)/He, 50 N cm^3 min^{-1}, 750 h^{-1} and 0.36 $g_{biomass+catalysts}$ h mol^{-1}) were performed at isothermal regime from 400 to 700 °C in 100 °C increments, following the same protocol: ramp from room temperature to the operating temperature and, after reaching the final temperature, the gases (dry basis) are analyzed at regular intervals up to 80 min of reaction. In these experiments, the Ni–Pt catalyst was also considered in the whole process and catalyst to biomass ratio was chosen to be 1/10. First, the mixed gasification of biomass occurred and then gas passed through the catalyst.

Fig. 4 represents gas product distribution at 600 °C during reaction time (25, 60 and 80 min). Below 30 min, H_2, CO, CO_2, CH_4, C_2H_6 and C_2H_4 are detected according to the stages taking place in the

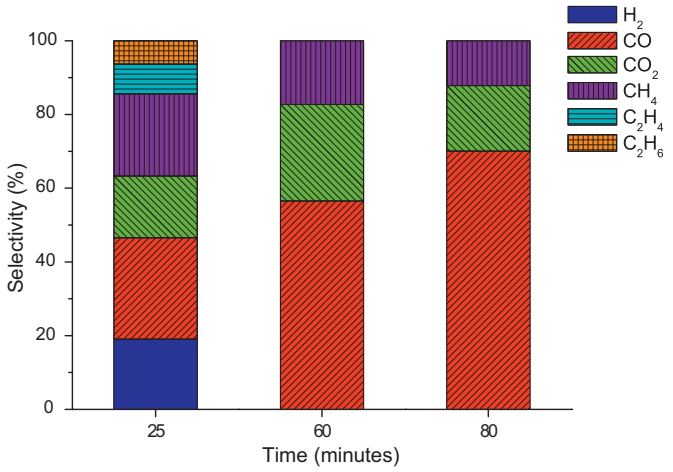

Fig. 4. Catalytic performance in $H_2O + CO_2$/He gasification of Sc biomass over the $Pt–Ni/Al_2O_3$ in the two stage fixed bed at 600 °C. Effect of time of reaction.

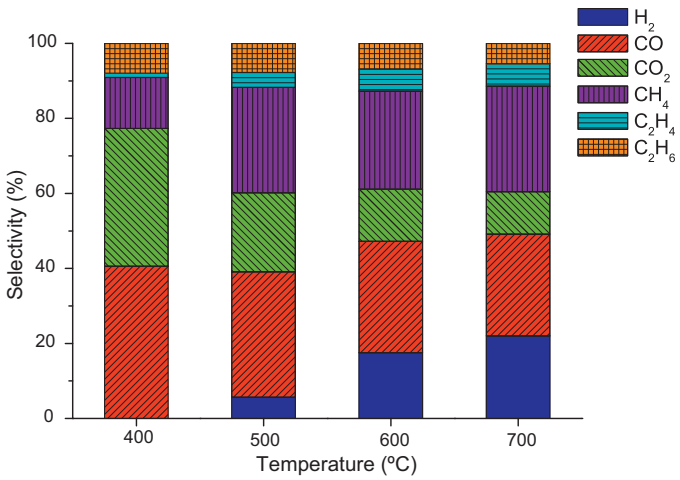

Fig. 5. Catalytic performance in $H_2O + CO_2$/He gasification of Sc biomass over the Pt–Ni/Al_2O_3 in the two stage fixed bed at 25 min of reaction time. Effect of reaction temperature.

catalytic gasification described above. After 60 min the selectivity is directed to CO, CO_2 and CH_4. After 80 min the amount of CO in the flue gas increased. These facts suggest the occurrence of further reforming reactions in the catalytic section of the devolatilized biomass that come from pyrolysis section; both with steam (Eq. (12)) and with CO_2 (Eq. (11)), the Boudouard reaction (Eq. (8)), methanations and the water–gas shift reaction (Eq. (10)). However, reforming reaction and WGS also produce hydrogen but after 60 min of reaction time hydrogen is not detected possibly because the contribution of Boudouard and water gas reaction have a prevailing role which would cause such a deviation in the content of CO_x [34].

Higher heating value (HHV) of gas was calculated according to the following correlation reported in [35]:

$$\mathrm{HHV} = \frac{12.63 \cdot [\mathrm{CO}] + 12.75 \cdot [\mathrm{H_2}] + 39.82 \cdot [\mathrm{CH_4}] + 63.43 \cdot [\mathrm{C_nH_m}]}{100}$$

where $[H_2]$, [CO], $[CH_4]$ and $[C_nH_m]$ are the molar fractions of H_2, CO, CH_4 and C_nH_m in the produced gas stream. Calculated HHV of produced gases at different time of reaction (25, 60 and 80 min) are 23.89, 14.01 and 13.68 MJ Nm^{-3}, respectively. These results indicate that a reaction time of 25 min is the most suitable under our current reaction conditions, since it allows to obtain a useful fuel gas free of condensable and tars adequate for fueling to static engines. So, 25 min was set to address the study of the influence of the temperature on the pyrolysis–gasification.

The effect of temperature on the gas composition with the presence of the catalyst is shown in Fig. 5. Major gases (H_2, CO, CO_2, C_2H_6 and C_2H_4) selectivity was affected by temperature. At 400 °C main pyrolysis occurred (Fig. 1) and CO_2 is majorly produced according to that discussed in Section 3.1. Furthermore, high temperature favors the products in endothermic reactions and the reactants in the exothermic reactions. Therefore, the products of intensive endothermic reactions and the reactants of exothermic reaction facilitated to be generated with temperature rising (Table 1). As observed, an increase in temperature enhances hydrogen formation due to the endothermic nature of the reactions involved: biomass pyrolysis (Eq. (1)), char reforming (Eqs. (8) and (9)), tar cracking and reforming (Eqs. (2) and (3)) and methane reforming. The concentration of CO decreases as temperature is increased and so the H_2/CO ratio (Table 4) increases from 0.17 to 0.81 at 500 °C and 700 °C, respectively, suggesting that above 700 °C a gas stream with a H_2/CO ratio near 1 could be achieved, which would not only use as fuel gas, but also for oxo-synthesis processes. Above 600 °C,

Table 4
Effect of catalytic gasification temperature in the H_2/CO, CO/CO_2 and HHV after 25 min of time of reaction. Reaction conditions: Pt–Ni/Al_2O_3, 750 h^{-1} and 0.36 $g_{biomass+catalysts}$ h mol^{-1}.

	400 °C	500 °C	600 °C	700 °C
H_2/CO	–	0.17	0.58	0.81
CO/CO_2	1.11	1.59	2.14	2.41
HHV (MJ Nm^{-3})	16.31	23.58	24.61	24.67

the effect of temperature on CO_2, CH_4 and C_2 hydrocarbon is not considerable. The increase in the CO/CO_2 molar ratio from 1.11 to 2.40 (net value), affecting also to the HHV, indicates the existence of subsequent char gasification reactions.

As was reported by several authors [36], the yield of liquid products and char decreases with increasing temperature once the temperature exceeds 400 °C because part of the volatiles forming the bio-oil cracked or reacts into more incondensable products and char decomposed at higher temperatures, this was confirmed by gravimetry. Williams and Nugranad [37] also reported that coke formation on ZSM-5 surface decreased at 600 °C in the pyrolysis of rice husk. After experimental runs at 700 °C, undecomposed tarry materials adhering to the wall of the reactor and in the trap were observed. Data from elemental analysis (CNHOS) showed a high carbon and oxygen content (64.9 and 14.23 wt.%, respectively) in the tarry material, after water elimination, suggesting the presence of heavy components. High nitrogen content (12.52 wt.%) could derived from the protein and chlorophyll of algal residues. S content was negligible, as it was released in the form of non-condensable gases. The results from the ultimate analysis of the char is given in Table 5. C, H, N and O contents decrease in the remaining solid fraction with increasing reaction temperature as the result of the gasification reaction between the solid fraction carbonaceous resulting from the pyrolysis, and the steam and/or carbon dioxide used as gasifying agent. In the experiments the char did not contact with the catalysts so char yield and composition is only dependent on the reaction temperature. Additionally, the ash content reached 80 wt.% after gasification of Sc biomass at 700 °C.

The use of Pt–Ni catalyst promotes, by mixed gasification $H_2O + CO_2$/He in the low temperature range (600–700 °C), the reforming reactions of the pyrolysis gases, the RWGS and parallel processes of cracking, by the gasification of heavy products and the char (for H_2O and CO_2) which globally causes higher gas yield, reaching a value close to 0.3 Nm^3 of gas per kg of biomass fuel diminishing the residual solid and condensable fraction in comparison with Nickel based catalysts.

As it is well known, the deactivation of nickel based catalysts in biomass gasification is the major drawback, owing to three main causes: sulphur poisoning, coke deposition (mainly from tar), and sintering [38]. However, for the Pt modified alumina supported catalyst, the Ni species have a high reducibility and is stabilized by the presence of Ni–Pt centers, this alloy is sulphur resistant and is not readily deactivated by coke formation improving further secondary reactions in the catalytic section. In addition, Pt and Rh are also well known for its ability to reduce carbon formation and deposition. We

Table 5
CHNOS (wt.%) and ash content in the solid residue according to the reaction temperature after isothermal analysis. Reaction conditions: t = 25 min, Pt–Ni/Al_2O_3, 750 h^{-1} and 0.36 $g_{biomass+catalysts}$ h mol^{-1}.

Temperature (°C)	C	H	N	S	O	Ash
400	37.41	2.11	5.87	–	19.68	34.93
500	18.12	0.76	2.97	0.02	9.71	68.42
600	15.30	0.25	1.95	–	8.62	73.88
700	12.72	–	1.46	–	7.63	78.19

analyzed Pt–Ni/Al_2O_3 catalyst after Sc biomass gasification under $H_2O + CO_2$/He atmosphere and by means of different characterization techniques and from XPS and FT-Raman we found a 40% of carbon content of amorphous nature and no S were detected. It is possible to produce a H_2 rich gas stream (>20 MJ Nm^{-3}, free of condensable) by catalytic pyrolysis–gasification at low temperature from the Sc microalgae biomass.

4. Conclusion

The effect of different gasifying agents on the product gas distribution was investigated in a thermobalance coupled to a MS. Major pyrolysis of Sc biomass occurs from 200 to 500 °C with independence of gasifying agent. Water vapor in the feed promotes reforming, water gas and water gas shift reaction improving H_2 in gas product distribution. The introduction of a Ni-based catalyst in a second bed upstream has been shown to be very active in the cracking and reforming of biomass volatiles and tars release during pyrolysis at low relatively temperature (600–700 °C) using $H_2O + CO_2$/He. Pt–Ni/Al_2O_3 allows to obtain 0.3 Nm^3 per kg of biomass of hydrogen enriched gas, at temperatures below 700 °C and a heating value near the 25 MJ Nm^{-3}.

Acknowledgements

The author want to acknowledge to the Spanish Ministry of Economy and Competitiveness the Financial support of PRI-PIBAR 2011-1343 and FYBOA group from the Department of Ecology of the University of Malaga for supplying the *Scenedesmus almeriensis* microalgae. MCR to the Spanish Ministry of Education, Culture and Sport (FPU12/03826) for FPU grant.

References

[1] M. Debowski, M. Zielinski, A. Grala, M. Dudek, Renew. Sustain. Energy Rev. 27 (2013) 596–604.
[2] S. Mandal, N. Mallick, Appl. Microbiol. Biotechnol. 84 (2009) 281–291.
[3] L. Lardon, A. Hélias, B. Sialve, J.P. Steyer, O. Bernard, Environ. Sci. Technol. 43 (17) (2009) 6475–6481.
[4] M.B. Johnson, Z. Wen, Energy Fuels 23 (10) (2009) 5179–5183.
[5] Y. Chisti, Biotechnol. Adv. 25 (2007) 294–306.
[6] R.P. Anex, A. Aden, F.K. Kazi, J. Fortman, R.M. Swanson, M.M. Wright, J.A. Satrio, R.C. Brown, D.E. Daugaard, A. Platon, G. Kothandaraman, D.D. Hsu, A. Dutta, Fuel 89 (2010) 529–535.
[7] F.Y.D. Yue, S.W. Snyder, Comput. Chem. Eng. (2013), http://dx.doi.org/10.1026/j.compchemeng.2013.11.016.
[8] A.B.Z. Alauddin, P. Lahijani, M. Mohammadi, A.R. Mohamed, Renew. Sustain. Energy Rev. 14 (9) (2010) 2852–2862.
[9] J.J. Hernández, G. Aranda, J. Barba, J.M. Mendoza, Fuel Process. Technol. 99 (2012) 43–55.
[10] S. Luo, B. Xiao, Z. Hu, S. Liu, X. Guo, M. He, Int. J. Hydrogen Energy 34 (2009) 2191–2194.
[11] L. Devi, K.J. Ptasinski, F. Janssen, Biomass Bioenergy 24 (2003) 125–140.
[12] S. Li, Y. Lu, L. Guo, X. Zhang, Int. J. Hydrogen Energy 22 (2011) 14391–14400.
[13] L. Wang, D. Li, H. Watanabe, M. Tamura, Y. Nakagawa, K. Tomishige, Appl. Catal. B: Environ. 5 (2014) 82–92.
[14] J. Wang, B. Xiao, S. Liu, Z. Hu, P. He, D. Guo, M. Hu, F. Qi, S. Lu, Bioresour. Technol. 103 (2013) 127–133.
[15] M. Asadullah, T. Miyazawa, S. Ito, K. Kunimori, K. Tomishige, Appl. Catal. A: Gen. 16 (2003) 246.
[16] N. Mahinpey, P. Murugan, T. Mani, R. Raina, Energy Fuels 23 (2009) 2736–2742.
[17] B.H.A. Sluiter, R. Ruiz, C. Scarlata, J. Sluiter, D. Templeton, Determination of Ash in Biomass, Technical Report NREL/TP-510-42622, National Renewable Energy Laboratory, 2008.
[18] K. Kebelman, A. Hornung, U. Karsten, G. Griffits, Biomass Bioenergy 49 (2013) 38–48.
[19] M. García-Diéguez, I.S. Pieta, M.C. Herrera, M.A. Larrubia, L.J. Alemany, J. Catal. 270 (2010) 136–145.
[20] M. García-Diéguez, I.S. Pieta, M.C. Herrera, M.A. Larrubia, L.J. Alemany, Catal. Today 172 (2011) 136–142.
[21] M. García-Diéguez, E. Finocchio, M.A. Larrubia, L.J. Alemany, G. Busca, J. Catal. 274 (2010) 11–20.
[22] S. Thangalazhy-Gopakumar, S. Adhikari, S.A. Chattanathan, R.B. Gupta, Bioresour. Technol. 118 (2012) 150–157.
[23] L. Sánchez-Silva, D. López-González, A.M. García-Mingillán, J.L. Valverde, Bioresour. Technol. 130 (2013) 321–331.
[24] A. Agrawal, S. Chakrabotty, Bioresour. Technol. 128 (2013) 72–80.
[25] A. Marcilla, A. Gómez-Siurana, C. Gomis, E. Chápuli, M.C. Catalá, F.J. Valdés, Thermochim. Acta 484 (2009) 41–47.
[26] N.H. Florin, A.T. Harris, Chem. Eng. Sci. 63 (2008) 287–316.
[27] H. Zhang, R. Xiao, D. Wang, G. He, S. Shao, J. Zhang, Z. Zhong, Bioresour. Technol. 102 (2011) 4258–4264.
[28] W.H. Chen, B.J. Lin, Appl. Energy 101 (2013) 551–559.
[29] B. Prabowo, K. Umeki, M. Yan, M.R. Nakamura, M.J. Castaldi, K. Yoshikawa, Appl. Energy 113 (2014) 670–679.
[30] M.P. Aznar, J. Corella, J. Delgado, J. Lahoz, Ind. Eng. Chem. Res. 32 (1993) 1.
[31] M.F. Irfan, M.R. Usman, K. Kusakabe, Energy 36 (2011) 12–40.
[32] S.Y. Zhang, J. Wang, J. Cao, T. Takarada, Bioresour. Technol. 102 (2011) 7561–7566.
[33] J. Nishiwaka, K. Nakamura, M. Asadullah, T. Miyazawa, K. Kunimori, K. Tomishige, Catal. Today 131 (2008) 146–155.
[34] C. Yang, L. Jia, S. Su, Z. Tian, Q. Song, W. Fang, C. Chen, G. Liu, Bioresour. Technol. 110 (2012) 676–681.
[35] Q. Xie, S. Kong, Y. Liu, H. Zeng, Bioresour. Technol. 110 (2012) 603–609.
[36] P. Pan, C. Hu, W. Yang, Y. Li, L. Dong, L. Zhu, D. Tong, R. Qing, Y. Fan, Bioresour. Technol. 101 (2010) 4593–4599.
[37] P.T. Williams, N. Nugranad, Energy 25 (2000) 493–513.
[38] J. Li, B. Xiao, R. Yan, X. Xu, Bioresour. Technol. 100 (2009) 5295–5300.